Superconductivity in the $Ba_{24}Si_{100}$ cubic clathrate with sp^2 and sp^3 silicon bondings

2005 J. Phys.: Condens. Matter 17 L311

(http://iopscience.iop.org/0953-8984/17/29/L01)

INSTITUTE OF PHYSICS PUBLISHING JOURNAL OF PHYSICS: CONDENSED MATTER

J. Phys.: Condens. Matter **17** (2005) L311–L319 doi:10.1088/0953-8984/17/29/L01

LETTER TO THE EDITOR

Superconductivity in the $Ba_{24}Si_{100}$ cubic clathrate with sp^2 and sp^3 silicon bondings

R Viennois[1], P Toulemonde[1], C Paulsen[2] and A San-Miguel[1]

[1] Laboratoire de Physique de la Matière Condensée et Nanostructures, Bâtiment Léon Brillouin, Université Claude Bernard Lyon I and CNRS, F-69622 Villeurbanne cedex, France
[2] Centre de Recherche sur les Très Basses Températures, CNRS, 25 avenue des Martyrs, F-38042 Grenoble cedex 9, France

Received 26 April 2005, in final form 23 June 2005
Published 8 July 2005
Online at stacks.iop.org/JPhysCM/17/L311

Abstract

In this letter, we report on the superconductivity of the type III helical cubic clathrate $Ba_{24}Si_{100}$. The onset of the superconducting transition is observed at $T_c = 1.55 \pm 0.05$ K. This is the first observation of a Si-based superconductor having both sp^2 and sp^3 bondings. The magnetic superconducting state is investigated from the determination of the critical fields H_{c1} and H_{c2} by ac susceptibility measurements. We find that $Ba_{24}Si_{100}$ is a type II superconductor with moderate electron–phonon coupling. The comparison with the other superconducting clathrate Ba_8Si_{46}, based only on sp^3 silicon atoms and which superconducts at 8 K, points out that the presence of sp^2 Si bondings in $Ba_{24}Si_{100}$ is an important parameter to take into account for explaining the moderate electron–phonon coupling and the lower superconducting critical temperature in $Ba_{24}Si_{100}$.

(Some figures in this article are in colour only in the electronic version)

In 1965, Cros *et al* [1, 2] discovered new allotropic forms of Si composed of nanocages allowing for the intercalation of alkaline elements: the clathrate compounds. Two different kinds of clathrate structures were found: the type I (e.g.: Na_8Si_{46}) and the type II structure (e.g.: Na_xSi_{136} with $0 \leqslant x \leqslant 24$). The unit cell of the first structure is composed of two cages of Si_{20} and six cages of Si_{24}, while the unit cell of the second one is composed of 16 Si_{20} cages and eight Si_{28} cages. Guest atoms (Na, K, Rb, I, . . .) are endohedrally intercalated in the silicon cages. These compounds can be viewed as an expanded sp^3 silicon network including a high density of pentagonal cycles (up to 87%). This predominance of odd cycles gives rise to a narrower electronic density of states (DOS) and phonon DOS compared with the case of diamond Si [3–5].

Over the past few years, compounds with clathrate structures have been the focus of much attention due to their good thermoelectric properties [6], their promising mechanical properties [7], their potential for optoelectronic applications correlated to their wide

bandgap [8] and the recent discovery of superconductivity in type I Ba intercalated Si clathrates [9–11], with a maximum superconducting critical temperature obtained for pure Ba_8Si_{46} ($T_c \cong$ 8–9 K) [10]. The discovery of a superconducting transition in these doped column-IV sp^3 semiconductors bears much analogy with the superconducting transition in boron-doped diamond [12, 13].

Only recently, the full intercalation of Ba in type I Si-based clathrate compounds has been achieved under high pressure (3 GPa) and high temperature (HP–HT) conditions (800 °C) [10, 11]. At lower pressure, around 1.5 GPa and high temperature, a new type of clathrate (type III)[3], $Ba_{24}Si_{100}$, was also obtained [14], which is isotypic with $Ba_{24}Ge_{100}$ [16].

This new type of clathrate structure is closely related to the type I structure as shown in figure 3 of [16]. The unit cell contains three different kinds of cages surrounding the Ba guest atoms: eight 'closed' Si_{20} cages, twelve 'open' Si_{20} cages and four cages composed of eight silicon atoms [14, 16]. It should be noted that the Si atoms forming this last class of cages have sp^2 bonding. Therefore in each unit cell 68 Si atoms have sp^3 bonding while 32 Si atoms have sp^2 bonding. Thus, contrary to the type I clathrate which is only composed of sp^3 silicon atoms, this type III clathrate structure possesses both sp^2 and sp^3 bondings.

Because superconductivity with strong covalent bonding is atypical, the study of such kinds of superconducting compounds is of great interest [11, 17, 18]. Within this class of compounds, we find the alkali-doped fullerenes, MgB_2 or the highly B-doped diamond [12, 13] and Si-based superconductors.

Among the Ba-based silicide compounds, it should be noted that only type I Ba-based clathrate compounds [9–11] and the metastable trigonal phase of $BaSi_2$ (synthesized under high temperature–high pressure conditions) are superconducting [19] and both possess a sp^3 Si lattice. The two other forms of $BaSi_2$, the orthorhombic and the cubic ones, have sp^2 Si bonds, are n-type semiconductors and do not superconduct [19–21].

Among the other Si-based superconducting phases, only $CoSi_2$ contains sp^3 Si bonds [22, 23], while other phases are based on Si sp^2 bonding schemes [21, 24–26]. Indeed, this is notably the case for $LaSi_2$ [25], the various superconducting phases of $CaSi_2$ [21] and the high pressure crystallographic forms of silicon [24]. The case of hexagonal $NbSi_2$ and $TaSi_2$ is still unclear although these phases seem to have silicon sp^2 bondings [21, 26]. The case of V_3Si is different, giving the fact that the appearance of superconductivity is essentially due to the high density of states at the Fermi level coming from the vanadium atoms [21].

Recently, superconductivity has been found in an isostructural compound of $Ba_{24}Si_{100}$, namely $Ba_{24}Ge_{100}$ (called Ba_6Ge_{25} in [27]) at about 0.24 K [27]. The study of this compound under pressure reveals an anomalous increase of T_c up to 3.8 K at a pressure of 2.8 GPa. However, in the first study of $Ba_{24}Si_{100}$, no superconducting transition has been found down to 2 K [14]. Very recently, a note (note 25 of [28]) in a paper concerning a Raman spectroscopy study of $Ba_{24}Si_{100}$ under high pressure reports superconductivity in this type III clathrate at 1.4 K [28].

In this letter, we confirm the existence of type II superconductivity with $T_c = 1.55 \pm 0.05$ K in $Ba_{24}Si_{100}$. The superconductivity phase diagram has been determined, i.e. the temperature dependence of the two critical fields H_{c1} and H_{c2}. To our knowledge, this is the first Si-based superconductor having both sp^2 and sp^3 bondings.

Powder mixtures of $BaSi_2$ (CERAC, 98%) and Si (Aldrich 99.9995%) corresponding to a $Ba_{24}Si_{100}$ composition were treated in a high pressure belt-type apparatus. The powders were mixed together and then compacted in small pellets (4 mm diameter) and placed inside a closed

[3] Two different notations have been proposed for $Ba_{24}Si_{100}$ and its isotypes: type III [14] and type I′ or IX [15]. We have chosen to follow the type III one to emphasize the analogies with the type I and II clathrates.

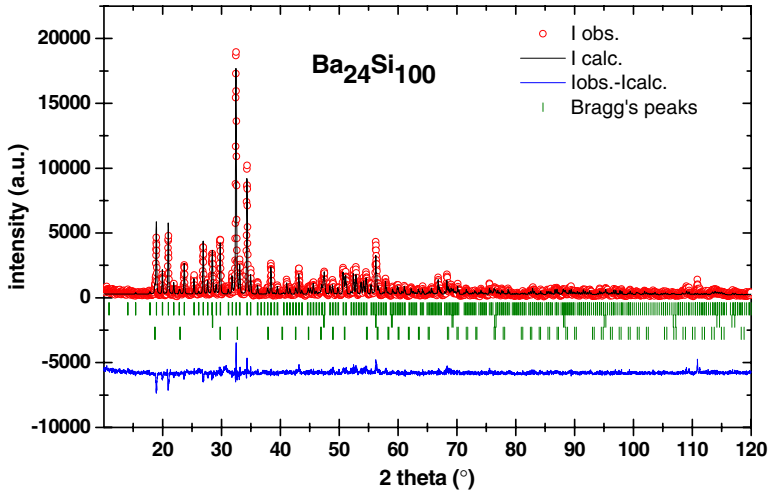

Figure 1. Experimental XRD pattern of $Ba_{24}Si_{100}$ (symbols) at room temperature. The black solid line is the Rietveld fitting using the structural model proposed by Fukuoka *et al* [14] and considering the presence of 6% in mass of cubic $BaSi_2$ and 7% of Si. The lower solid line is the difference curve (observed minus calculated). Tick marks correspond to Bragg reflections of $Ba_{24}Si_{100}$ (first row), Si (second row) and $BaSi_2$ (third row).

h-BN crucible which was introduced inside a graphite tube furnace. The whole assembly was then inserted in the pyrophyllite high pressure gasket. The HP–HT synthesis was performed under a pressure of 1.1 GPa at 650 °C for 1 h. This synthesis temperature is lower than the one in [14] (800 °C). We observe that in such a case, (i) the pressure domain of the synthesis is narrower than at 800 °C and (ii) the amount of secondary phases is higher at 650 °C than at 800 °C. If the pressure is slightly increased to 1.2–1.3 GPa, an additive impurity phase appears: the type I clathrate Ba_8Si_{46}. X-ray diffraction (XRD) patterns were collected using a Siemens D-500 powder diffractometer working in Bragg–Brentano geometry at the $K\alpha_{1,2}$ Cu wavelengths from $2\theta = 10°$ to 120° with a step of 0.02°. From the Rietveld refinement of the x-ray diffraction (XRD) pattern (figure 1), we have determined that our samples contain about 7% in mass of Si and 6% of cubic $BaSi_2$. The cubic lattice parameter for our $Ba_{24}Si_{100}$ sample has been found to be equal to 14.0630(±0.0003) Å, which is close to 14.0685 Å found by Fukuoka and co-workers [14]. It should be noted that both impurity phases are not superconducting at room pressure [19, 20, 24].

Investigation of the superconducting properties of $Ba_{24}Si_{100}$ was performed using two low temperature SQUID magnetometers developed at the CRTBT in Grenoble. A bulk polycrystalline $Ba_{24}Si_{100}$ sample of about 5.6 mg mass with fine grains was studied. The form of the sample was roughly a half-disc, and measurements were made parallel to the long axis. We estimate the demagnetization factor 'N' for this direction to be about 1–2 in CGS units. For the temperature-dependent magnetic measurements, both magnetization (M) with 5 Oe magnetic field (H) and ac magnetic susceptibility χ_{ac} were measured. We used a frequency of 1.1 Hz and field less than 1 Oe for the χ_{ac} measurements.

To determine the superconducting critical fields H_{c1} and notably H_{c2}, the field dependence of the magnetization was measured. However, magnetization measurements at high magnetic fields were too noisy to permit us to determine H_{c2}. Therefore, in order to have better precision for allowing the determination of H_{c2} without ambiguity, we performed field dependent measurements of χ_{ac} between $T = 0.075$ and 1.4 K.

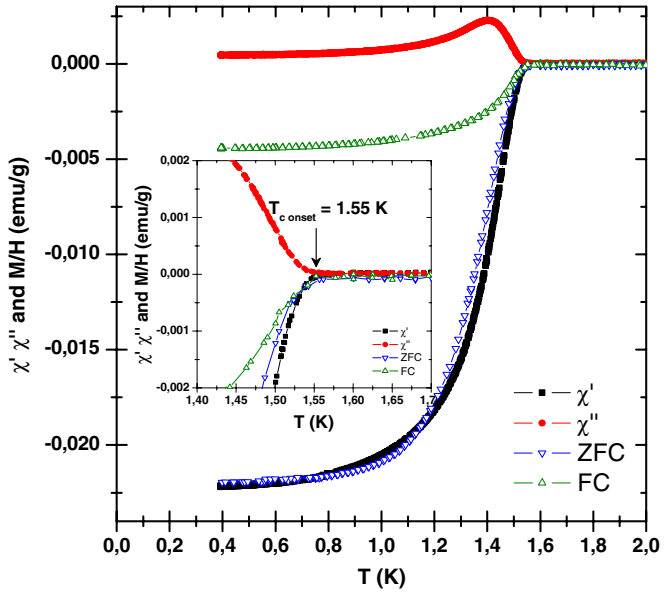

Figure 2. Thermal variation of the dc magnetization M and of the ac magnetic susceptibility χ_{ac}. The dc magnetization has been measured both with zero-field cooling (ZFC) and with field cooling (FC) procedures. χ' and χ'' are respectively the real and the imaginary parts of χ_{ac}. The onset of the superconducting transition is shown in the inset.

From the thermal variation of the magnetization measured in a 5 Oe magnetic field and of χ_{ac} (figure 2), a huge drop of the diamagnetic susceptibility is observed below 1.55 K. This is the signature of a superconducting transition with a critical onset temperature at $T_c = 1.55 \pm 0.05$ K (see the inset of figure 2). This value is a little bit higher than the 1.4 K value reported by Tanigaki *et al* evoked in note 25 of [28]. This slight difference of 0.15 K between both T_c values could be explained by very small differences in Ba contents between the two $Ba_{24}Si_{100}$ samples. Indeed, similar behaviour has been observed in Ba_8Si_{46} for which the presence of Ba vacancies in the small Si_{20} cages implies a decrease of its T_c [29]. Within a standard BCS approach to superconductivity, usually used for all the Si-based superconductors, we can deduce the value of the superconducting gap at 0 K from the critical temperature T_c using the well known relation [30] $2\Delta\ (T \to 0\ \mathrm{K}) = 3.52\, k_B T_c$. We find $\Delta\ (T \to 0\ \mathrm{K}) = 0.235$ meV. Tunnelling experiments are under way for checking this estimation of the value of the superconducting gap.

The field-cooled (FC) magnetization shows a relatively large flux expulsion (Meissner effect) of nearly 18%. Evidence of the type II superconducting state can be seen in figure 3 where we have plotted M versus H for $T = 75$ and 400 mK. At small fields, shielding is 100% and M versus H is approximately linear. At large fields, flux penetrates in the form of vortices and $|M|$ decreases. At 400 mK, we estimate H_{c1} as the field where flux first penetrates into the sample, and the magnetization departs from linearity which occurs at an applied field of approximately 9 ± 1 Oe, as seen in the inset of figure 3. Thus, this gives a value of H_{c1} of approximately 12 ± 2 Oe for the extrapolation at $T = 0$ K, when corrections are made for demagnetization effects.

The value of the zero-field-cooled magnetization (ZFC) measured at 0.4 K is very close to the one expected if the entire sample is supposed to be superconducting (figure 2). Indeed, for a perfect diamagnetic compound, we have $\chi = -1/(4\pi - N)$ emu cm^{-3} and therefore we expect

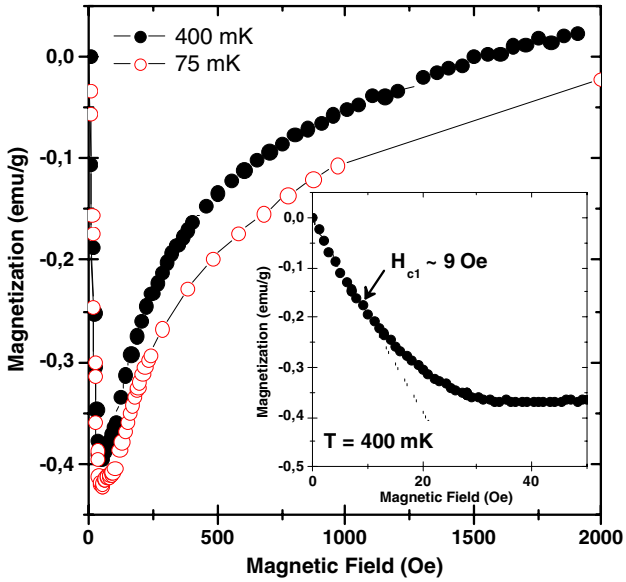

Figure 3. Field variation of the dc magnetization for $T = 75$ and 400 mK. Inset: close-up view of the field variation of the dc magnetization at low magnetic field for $T = 400$ mK (second set of measurements at 400 mK with a smaller magnetic field step). The lower critical field H_{c1} is determined from the departure from linearity at low field, which occurs at an applied field of approximately 9 Oe. When corrections are made for demagnetization effects, we estimate H_{c1} to be approximately 12 Oe for $T \to 0$ K.

χ to lie between -0.086 (for $N = 1$) and -0.094 emu cm^{-3} (for $N = 2$). From the comparison with the experimental value $\chi = -0.08$ emu cm^{-3} (with a $Ba_{24}Si_{100}$ density of 3.64 g cm^{-3}), we can estimate that about 90% of the sample is superconducting, which is in good agreement with the XRD estimation of the $Ba_{24}Si_{100}$ content of our sample. Therefore, from the above considerations, we can unambiguously attribute this type II bulk superconductivity with a T_c onset at 1.55 ± 0.05 K to the $Ba_{24}Si_{100}$ clathrate phase.

In order to determine the upper critical field H_{c2}, the field dependence of the ac susceptibility has been measured for different temperatures: 0.075, 0.4, 0.8, 1, 1.1, 1.2, 1.3 and 1.4 K (for clarity, only some temperatures are shown in figure 4). In figure 4 (upper part), we have determined H_{c2} from the value of the magnetic field for which χ'', the imaginary part of χ_{ac}, collapses to zero. For $T = 75$ mK (not shown), we find $H_{c2} \cong 3500 \pm 200$ Oe. Thus, using this method for determining H_{c2} at each temperature, we obtain the temperature variation of H_{c2} shown in figure 5, which is the typical variation expected for a normal type II superconductor.

For temperature close to T_c, H_{c2} decreases almost linearly with temperature with a slope $H'_{c2} = -dH_{c2}/dT$ equal to 0.27 T K^{-1} for $Ba_{24}Si_{100}$ (figure 5) which is considerably smaller than $H'_{c2} \cong 1.5$–2.9 T K^{-1} found for the isostructural compound $Ba_{24}Ge_{100}$ [27]. Concerning the case of Ba_8Si_{46}, H'_{c2} is not known, but from $T_c = 8$ K and $H_{c2} = 6.5$ T determined for this compound [10, 31] we can reasonably estimate that $H'_{c2} \cong 0.8$–1 T K^{-1}. This is also much higher than for $Ba_{24}Si_{100}$.

From the estimates of H_{c1} and H_{c2}, we can determine the penetration depth λ and the coherence length ξ for $T \to 0$ K using the Ginzburg–Landau equations [32]:

$$\mu_0 H_{c2} = \phi_0/2\pi\xi^2 \tag{1}$$

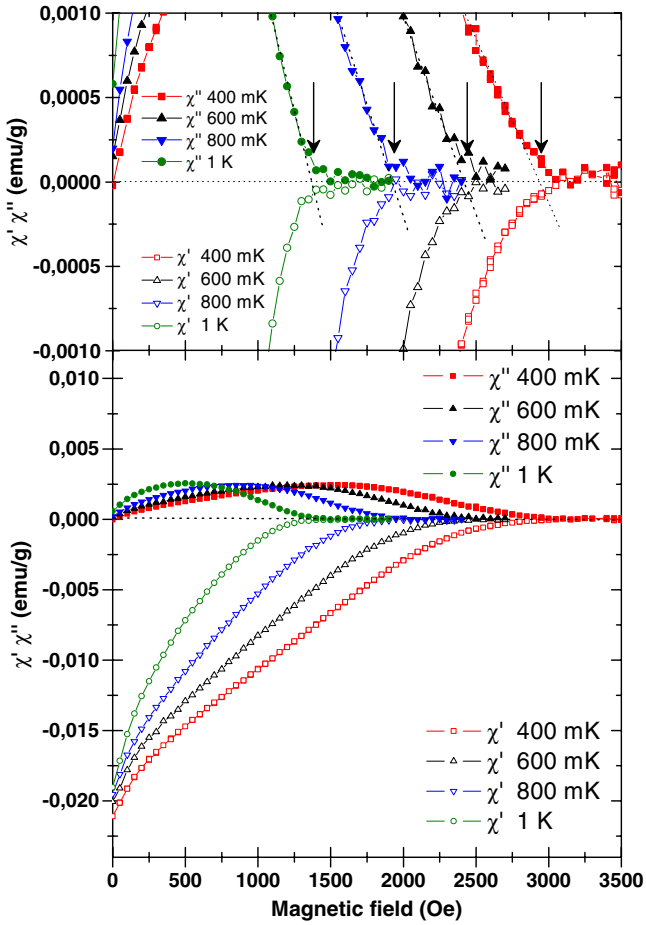

Figure 4. Bottom: field variation of the ac magnetic susceptibility χ_{ac} for different temperatures. Top: zoom showing the extrapolation to zero of the imaginary part of χ_{ac} used to determine the critical field H_{c2} (marked by vertical arrows).

and

$$\mu_0 H_{c1} = \phi_0 \ln(\kappa)/4\pi\lambda^2 \tag{2}$$

where $\kappa = \lambda/\xi$ is the Ginzburg–Landau parameter and $\phi_0 = \pi\hbar c/e$ is the quantum flux.

Thus, for $T \to 0$ K, from $H_{c1}(T \to 0\ \text{K}) \cong 12$ Oe and $H_{c2}(T \to 0\ \text{K}) \cong 3500$ Oe, we find $\lambda \cong 6500$ Å and $\xi \cong 310$ Å. Hence, we obtain $\kappa \cong 21$. These values can be compared with Ba_8Si_{46} where $\lambda \cong 4000$ Å, $\xi \cong 72$ Å and $\kappa \cong 56$ [31]. We have then for these two compounds the same order of magnitude for λ while ξ is four times smaller for Ba_8Si_{46}. We can also remark that in the isostructural compound $Ba_{24}Ge_{100}$ ξ is similar ($\xi \cong 280$–350 Å) [27] to the value for $Ba_{24}Si_{100}$.

In the framework of a BCS model for superconductivity, we can now estimate the electron–phonon coupling strength λ_{e-ph} in $Ba_{24}Si_{100}$ from the McMillan formula [33]:

$$T_c = (\theta_D/1.45)\exp(-1.04(1+\lambda_{e-ph})/\lambda_{e-ph} - \mu^*(1+0.62\lambda_{e-ph}))$$

where θ_D is the Debye temperature and μ^* is the effective electron–electron repulsive

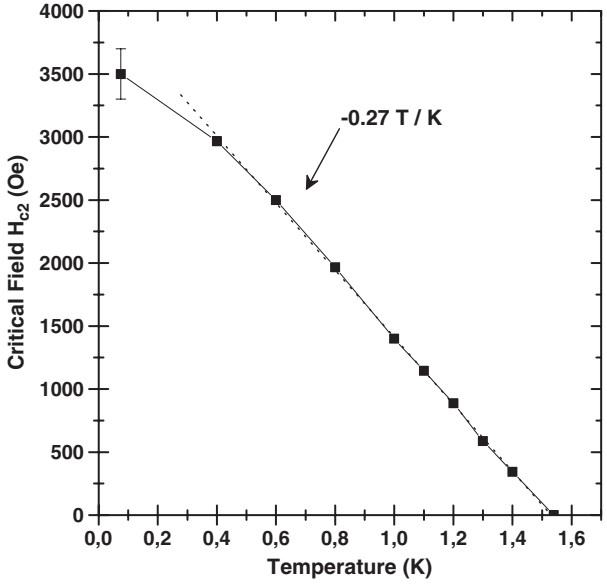

Figure 5. Temperature variation of the upper critical field H_{c2}.

Table 1. Fundamental superconducting parameters of barium-based type III and type I group IV clathrates. See the text for details.

Compound	T_c (K)	λ_{e-ph}	λ (Å)	ξ (Å)
Ba_8Si_{46} [17, 31]	8.0	1.05	4000	72
$Ba_{24}Si_{100}$ (This work)	1.55 ± 0.05	0.4–0.7	6500	310
$Ba_{24}Ge_{100}$ [27]	0.24	0.31	—	280–350

interaction. If we make the reasonable assumptions that θ_D is about 350–400 K[Note 4] and μ^* is comprised between 0.1 (value estimated for $Ba_{24}Ge_{100}$ [27]) and 0.24 (value estimated for Ba_8Si_{46} [17, 18]), we find that $\lambda_{e-ph} = 0.4$–0.7. This range for the electron–phonon coupling falls between the values found for $Ba_{24}Ge_{100}$ ($\lambda_{e-ph} = 0.31$ from [27]) and Ba_8Si_{46} ($\lambda_{e-ph} = 1.05$ from [17]), as is also the case for T_c. This means that both type III structure compounds, $Ba_{24}Si_{100}$ and $Ba_{24}Ge_{100}$, are in the moderate electron–phonon coupling regime ($Ba_{24}Ge_{100}$ being rather closer to the weak electron–phonon limit), compared to the type I structure of Ba_8Si_{46}, which shows a strong coupling. All these values are summarized in table 1. However, no further conclusion can be drawn due to the difference between the crystallographic structures of $Ba_{24}Si_{100}$ and Ba_8Si_{46}.

It has been already proposed that both the strong electron–phonon coupling inside the Si_{24} cages [5] and sp^3 bonding [17] were essential, in addition to the high electron density of states at the Fermi level, for explaining the superconducting properties of Ba_8Si_{46} and notably its relatively high T_c. In $Ba_{24}Si_{100}$, the Si_{24} cages, analogous to the ones of Ba_8Si_{46}, disappear to form cubic Si_8 cages composed of sp^2 silicon bonds and open Si_{20} cages [14]. To better understand the implication of the sp^2 bondings in the electron–phonon coupling and to confirm

[4] Our assumption seems reasonable because the phonon modes experimentally measured by Raman spectroscopy are in the same frequency range in Ba_8Si_{46} and in $Ba_{24}Si_{100}$; moreover, $\theta_D = 370$ K in Ba_8Si_{46} (evaluated by specific heat measurements, see [18]); therefore, θ_D should have the same magnitude in $Ba_{24}Si_{100}$. Note also that the estimation of λ_{e-ph} from T_c using the McMillan formula is not very sensitive to the value of θ_D.

the weaker electron–phonon coupling in $Ba_{24}Si_{100}$ compared to Ba_8Si_{46}, further studies would be of great interest. This will help us to understand the superconducting properties in both silicon clathrate systems: the sp^3 case of Ba_8Si_{46} and the mixed sp^2/sp^3 case of $Ba_{24}Si_{100}$.

On the other hand, in the carbon-based superconductors, it seems that the most important effect explaining the T_c evolution between sp^2 and sp^3 systems (considering the same density of states at the Fermi level) is the larger electron–phonon coupling in the sp^3 C-diamond case compared to the sp^2 graphite case [13]. Thus, our results on the silicon system point out the importance of the dominance of sp^3 bonding in the quest for new carbon nanocage-based superconductors with potential high critical superconducting temperatures [7, 17].

In summary, in this letter, we report on the superconductivity of the type III helical cubic clathrate $Ba_{24}Si_{100}$. The onset of the superconducting transition occurs at $T_c \cong 1.55$ K. This is the first observation of a Si-based superconductor having both sp^2 and sp^3 bondings. The investigation of the magnetic superconducting state shows that $Ba_{24}Si_{100}$ is a type II superconductor. The critical magnetic fields H_{c1} and H_{c2} were measured to be $H_{c1}(0\ \mathrm{K}) \cong 12$ Oe and $H_{c2}(0\ \mathrm{K}) \cong 3500$ Oe. The London penetration depth λ ($\sim$6500 Å) has the same order of magnitude as the one determined for Ba_8Si_{46}, while the coherence length ($\sim$310 Å) is smaller in $Ba_{24}Si_{100}$ than in Ba_8Si_{46}, and is closer to that found in the isotypic $Ba_{24}Ge_{100}$ compound. Our estimate of the electron–phonon coupling reveals that $Ba_{24}Si_{100}$ is a moderate phonon-mediated BCS superconductor.

This work was supported by the French Ministère Délégué à la Recherche et aux Nouvelles Technologies grants ACI-2003 No NR0122 and ACI-2003 No JC2077, as well as by Université Claude Bernard Lyon I grant No BQR-2003. The authors wish to thank Dr X Blase, J-P Brison and A Sulpice for useful discussions and also R Vera, who made XRD measurements in the Centre de Diffractométrie Henri Longchambon at the University of Lyon.

Note added. Very recently, after submission of our letter, the group of Professor Tanigaki confirmed superconductivity at $T_c = 1.4$ K in $Ba_{24}Si_{100}$ by resistivity and specific heat measurements at the ISIC 13 conference, 6–9 June 2005, Clermont-Ferrand, France.

References

[1] Cros C, Pouchard M and Hagenmüller P 1965 *C. R. Acad. Sci. Paris* A **260** 4764
[2] Cros C, Pouchard M and Hagenmüller P 1970 *J. Solid State Chem.* **2** 570
[3] Mélinon P *et al* 1998 *Phys. Rev.* B **58** 12590
[4] Mélinon P *et al* 1999 *Phys. Rev.* B **59** 10099
[5] Reny E *et al* 2002 *Phys. Rev.* B **66** 014532
[6] Nolas G S *et al* 1998 *Appl. Phys. Lett.* **73** 178
[7] San Miguel A *et al* 2005 *Europhys. Lett.* **69** 556 and references therein
[8] Gryko J *et al* 2000 *Phys. Rev.* B **62** 7707
Connétable D, Timoshevskii V, Artacho E and Blase X 2001 *Phys. Rev. Lett.* **87** 206405
[9] Kawaji H, Hori H, Yamanaka S and Ishikawa M 1995 *Phys. Rev. Lett.* **74** 1427
[10] Yamanaka S, Enishi E, Fukuoka H and Yasukawa M 2000 *Inorg. Chem.* **39** 56
[11] Toulemonde P, Adessi C, Blase X, San Miguel A and Tholence J L 2005 *Phys. Rev.* B **71** 094504 and references therein
[12] Ekimov E A *et al* 2004 *Nature* **428** 542
[13] Blase X, Adessi C and Connétable D 2004 *Phys. Rev. Lett.* **93** 237004
[14] Fukuoka H, Ueno K and Yamanaka S 2000 *J. Organomet. Chem.* **611** 543
[15] Mudryk Ya, Rogl P, Paul C, Berger S, Bauer E, Hilscher G, Godart C and Noël H 2002 *J. Phys.: Condens. Matter* **14** 7991
[16] Fukuoka H, Iwai K, Yamanaka S, Abe H, Yoza K and Häming L 2000 *J. Solid State Chem.* **151** 117
[17] Connétable D *et al* 2003 *Phys. Rev. Lett.* **91** 247001
[18] Tanigaki *et al* 2003 *Nat. Mater.* **2** 653

[19] Imai M, Hirata K and Hirano T 1995 *Physica* C **245** 12
[20] Imai M, Hirano T, Kikegawa T and Shimomura O 1998 *Phys. Rev.* B **58** 11922
[21] Sanfilippo S *et al* 2000 *Phys. Rev.* B **61** 3800 and references therein
[22] Matthias B T 1952 *Phys. Rev.* **87** 380
[23] Tersoff J and Hamann D R 1983 *Phys. Rev.* B **28** 1168
[24] Chang K J *et al* 1985 *Phys. Rev. Lett.* **54** 2375
[25] Travlos A and Salamouras N 1997 *Vacuum* **48** 13
[26] Gottlieb U *et al* 1992 *Phys. Rev.* B **45** 4803
[27] Yuan H Q *et al* 2004 *Phys. Rev.* B **70** 174512 and references therein
Yuan H Q *et al* 2002 *J. Phys.: Condens. Matter* **14** 11249
[28] Shimizu H *et al* 2005 *Phys. Rev.* B **71** 094108
[29] Fukuoka H, Kiyoto J and Yamanaka S 2004 *J. Chem. Phys. Solids* **65** 333
[30] Bardeen J, Cooper L N and Schrieffer J R 1957 *Phys. Rev.* **108** 1175
[31] Gat I M *et al* 2000 *Physica* B **289/290** 385
[32] Ginzburg V L and Landau L D 1950 *Zh. Eksp. Teor. Fiz.* **20** 1064
[33] McMillan W L 1968 *Phys. Rev.* **167** 331